

Insertion Loss of Traction Inverter Electromagnetic Interference Filter as a Function of Noise Source Impedance

Róbert Orvai^{1,2}, Márk Csörnyei², János Hamar¹

¹*Budapest University of Technology and Economics, Department of Automation and Applied Informatics, Budapest, Hungary; orvai.robert@aut.bme.hu*

²*Robert Bosch Kft., Budapest, Hungary*

Abstract. The noise source impedance has a major impact on the insertion loss (IL) of the traction inverter electromagnetic interference filter in electric cars. It is possible to determine the source impedance conditions at which the IL will be minimum or maximum. This paper exploits this to present a method for identifying critical frequency ranges regarding the minimum IL when the information about the source impedance is limited. Thus, the expectable IL can be predicted before the exact source impedance is known, and responses to changes in the termination impedance can be made more efficient.

1 Introduction

The electromagnetic interference (EMI) filter on the DC side of the traction inverter in electric cars usually has only a few stages or orders due to the high voltage and current levels present. The fewer the stages of a passive EMI filter, the more dependent its insertion loss (IL) is on the termination impedances [1]. Therefore, the IL of these filters depends highly on the terminations, which property is accounted for in modern filter optimization methods [2]. The termination impedance on one side of the filter is well-known, which is the AC resistance of the line impedance stabilization network(s) (LISN) used in electromagnetic compatibility (EMC) testing. On the other side, however, the termination impedance depends on the inverter, the electric machine and the overall system (Fig. 1), i.e. the noise source. Its exact value cannot be known at every moment throughout the entire development process, since the filter is not only an electrical, but an electro-mechanical-thermal product. Thanks to the mentioned high voltage and current levels, the filter needs to meet severe mechanical a thermal requirements, and the modifications made for achieving these often results in the change of the termination impedance. This makes it difficult for the exact noise source impedance to be available all the time. Additionally, in a lot of cases the focus is on the magnitude of the source impedance only, which does not reflect the reality.

Hence, this paper attempts to study the dependence of the insertion loss of typical low-stage filter topologies on the complex noise source impedance at different frequencies. Furthermore, a graphical method is presented which can be used if the parameters of the filter are known but the information on the noise source impedance is only approximate. The method can identify critical frequency ranges at which the IL could differ heavily from its expected value measured in a 50 Ω system. In the second section, the general terms and equations are introduced which were used during the course of the study. Section 3 presents the calculation of the noise source impedance condition at which the insertion loss will be minimum or maximum along with illustrations. The graphical method which can be used for identifying the critical frequency ranges is introduced in the fourth section. Finally, Section 5 summarizes the conclusions of the work.

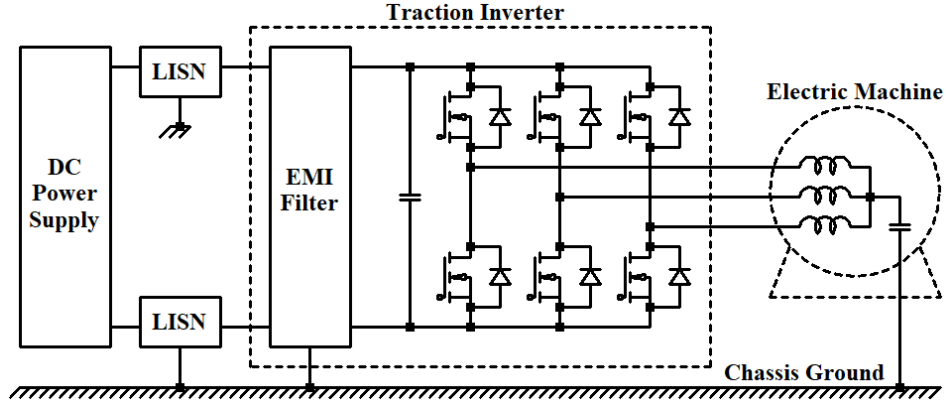


Figure 1: System diagram from an EMC point of view.

2 Mathematical Context

The EMI filter of traction inverters is a two-line filter forming a three-port network as depicted in the upper part of Fig. 2 (a) (the ground (G) in this case is the chassis of the car as indicated in Fig. 1). The filter can be divided into differential-mode (DM) and common-mode (CM) parts. The resulting two-port networks are easier to grasp from a mathematical point of view, because the insertion loss taking into account the termination impedances can be expressed using four two-port network parameters of arbitrary type [3]. In this problem area, the IL in decibels is written using the chain, cascade, transmission or ABCD-parameters:

$$IL = 20 \log_{10} \left| \frac{\overline{A} \overline{Z}_l + \overline{B} + \overline{C} \overline{Z}_s \overline{Z}_l + \overline{D} \overline{Z}_s}{\overline{Z}_s + \overline{Z}_l} \right| \quad (1)$$

Note that by definition, insertion loss is the ratio of power at the load before and after inserting a device into the system. In the context of EMI filters, IL is defined as the quotient of the voltage measured on the load before and after the insertion of the filter. This is a significant difference from the point of view that in terms of signal power, the insertion loss of a passive filter cannot be negative in decibels. In other words, a passive network cannot have power gain. However, defining IL in terms of chain parameters as in (1) allows it to take negative values in dB, because the formula is derived from the voltage ratio [4], and voltage gain can occur due to resonance.

In (1), \overline{Z}_s denotes the varying complex noise source impedance, and \overline{Z}_l is the complex load impedance from the LISN(s) as illustrated in Fig. 2 (b). In the following sections, using the algebraic form of the impedances, the real part is denoted by R and the imaginary part by X :

$$\overline{Z}_s = R_s + jX_s \quad \overline{Z}_l = R_l + jX_l \quad (2)$$

The also complex ABCD-parameters in (1) make up the chain parameter or transmission matrix (\mathbf{T}) of the studied two-port filter and it is defined as follows:

$$\mathbf{T} = \begin{bmatrix} \overline{A} & \overline{B} \\ \overline{C} & \overline{D} \end{bmatrix} \quad \begin{bmatrix} \overline{V}_1 \\ \overline{I}_1 \end{bmatrix} = \begin{bmatrix} \overline{A} & \overline{B} \\ \overline{C} & \overline{D} \end{bmatrix} \begin{bmatrix} \overline{V}_2 \\ \overline{I}_2 \end{bmatrix} \quad (3)$$

where \overline{V}_1 and \overline{I}_1 are the input voltage and current, \overline{V}_2 and \overline{I}_2 are the output voltage and current of the two-port network, respectively (Fig. 2 (b)).

For the rest of the study, the focus is on the CM part of the EMI filter. The CM part is a low-pass filter with a few stages consisting of series inductors (CM chokes) and parallel capacitors

(Y-capacitors). Such topologies are the L, C, LC (T), CL (Γ), LCL (T) and CLC (Π) filters (Fig. 3 (a)), whose \mathbf{T} -matrices, assuming that the values of the inductors and the capacitors are the same, are shown below:

$$\begin{aligned}\mathbf{T}_L &= \begin{bmatrix} 1 & \bar{Z}_L \\ 0 & 1 \end{bmatrix} & \mathbf{T}_C &= \begin{bmatrix} 1 & 0 \\ \bar{Y}_C & 1 \end{bmatrix} \\ \mathbf{T}_{LC} &= \begin{bmatrix} 1 + \bar{Z}_L \bar{Y}_C & \bar{Z}_L \\ \bar{Y}_C & 1 \end{bmatrix} & \mathbf{T}_{CL} &= \begin{bmatrix} 1 & \bar{Z}_L \\ \bar{Y}_C & 1 + \bar{Z}_L \bar{Y}_C \end{bmatrix} \\ \mathbf{T}_{LCL} &= \begin{bmatrix} 1 + \bar{Z}_L \bar{Y}_C & \bar{Z}_L^2 \bar{Y}_C + 2\bar{Z}_L \\ \bar{Y}_C & 1 + \bar{Z}_L \bar{Y}_C \end{bmatrix} & \mathbf{T}_{CLC} &= \begin{bmatrix} 1 + \bar{Z}_L \bar{Y}_C & \bar{Z}_L \\ \bar{Z}_L \bar{Y}_C^2 + 2\bar{Y}_C & 1 + \bar{Z}_L \bar{Y}_C \end{bmatrix}\end{aligned}\quad (4)$$

The transmission matrices of the topologies with higher number of stages can be obtained by performing the non-commutative matrix multiplication of the \mathbf{T}_L and \mathbf{T}_C matrices in the appropriate order. \bar{Z}_L above is the impedance of the series inductor, and \bar{Y}_C is the admittance of the parallel capacitor in the parameterized low-pass filter:

$$\bar{Z}_L = j2\pi fL \quad \bar{Y}_C = j2\pi fC \quad (5)$$

where f denotes the frequency. Also, \bar{Z}_L and \bar{Y}_C can be complemented with parasitics of the inductor and the capacitor [5]. The inductor can be modeled as a parallel RLC, and the capacitor as a series RLC network as shown in Fig. 3 (b). \bar{Z}_L and \bar{Y}_C in this case is as follows:

$$\bar{Z}_L = \frac{1}{\frac{1}{j2\pi fL} + j2\pi fEPC_L + \frac{1}{EPR_L}} \quad \bar{Y}_C = \frac{1}{\frac{1}{j2\pi fC} + j2\pi fESL_C + ESR_C} \quad (6)$$

where EPC_L and EPR_L are the equivalent parallel capacitance and resistance of the inductor, ESL_C and ESR_C are the equivalent series inductance and resistance of the capacitor, respectively. Having determined the terms used in the computations of the following sections, Section 3 will define and visualize the critical points of the insertion loss.

3 Noise Source Impedance at Which the Insertion Loss Will Be Minimum or Maximum

Assuming that the fixed load impedance is known because the impedance of the LISN is available as mentioned previously, the dependency of insertion loss on the noise source impedance can be provided. According to [6], the IL takes its minimum or maximum values at a certain frequency when the imaginary part of the source impedance is respectively $X_{s\min}$ or $X_{s\max}$, while its real part, R_s , is minimum. $X_{s\min}$ and $X_{s\max}$ can be calculated the following way, which formulas are the result of the minimum and maximum search of the insertion loss using derivatives:

$$X_{s\min} = \frac{-R_l^2 + R_{e1}^2 - X_l^2 + X_{e1}^2 + \sqrt{\Delta}}{2(X_l - X_{e1})} \quad (7)$$

$$X_{s\max} = \frac{-R_l^2 + R_{e1}^2 - X_l^2 + X_{e1}^2 - \sqrt{\Delta}}{2(X_l - X_{e1})} \quad (8)$$

where R_{e1} and X_{e1} are the real and imaginary parts of impedance \bar{Z}_{e1} introduced in [6] to shorten the otherwise long formulas for $X_{s\min}$ and $X_{s\max}$.

$$\bar{Z}_{e1} = \frac{\bar{A}\bar{Z}_l + \bar{B}}{\bar{C}\bar{Z}_l + \bar{D}} \quad (9)$$

The parameter Δ in (7) and (8) after performing the minimum and maximum search of the insertion loss expressed with the use of \bar{Z}_{e1} is

$$\Delta = (-R_l^2 + R_{e1}^2 - X_l^2 + X_{e1}^2)^2 - 4(-X_l + X_{e1})(X_l X_{e1}^2 - X_{e1}(R_l^2 + X_l^2) + R_{e1}^2 X_l) \quad (10)$$

To illustrate the minimum and maximum insertion loss where the imaginary part of the source impedance takes the value of $X_{s\min}$ or $X_{s\max}$, Fig. 4 shows the dependency of IL on \bar{Z}_s at different frequencies for an ideal LC filter without parasitics ($L = 10 \mu\text{H}$ and $C = 100 \text{nF}$). The load impedance was assumed to be $(25 + j0) \Omega$ from the LISNs in common mode. The computations were done in Python using the mathematical relationships presented in Section 1. The x- and y-axis in Fig. 4, on which the real and imaginary parts of the source impedance are indicated, are logarithmically scaled. For the negative values of X_s , symmetric logarithmic axis scaling was used [7]. Also, relatively wide ranges have been specified for R_s and X_s to capture the trends in the contour plots. It can be seen that the insertion loss takes its minimum and maximum values at every studied frequency indeed where the real part of the source impedance is minimum. This can be explained by the formulas for IL presented in [6], which imply that the insertion loss will be minimum if $R_s = -R_{e1}$ and $X_s = -X_{e1}$, and maximum if $R_s = -R_l$ and $X_s = -X_l$. But, because R_s cannot be negative, theoretically the minimum and maximum IL will be at $R_s = 0 \Omega$. Since the source impedance always has some ohmic resistance, the minimum and maximum of the insertion loss will be at minimum R_s . The X_s values indicated in red at these points were calculated separately using expressions (7)-(10) above. It can also be deduced from the figures that if the real part of the source impedance is sufficiently large, the imaginary part has no effect on the insertion loss. These R_s values are indicated with vertical black lines, at which the variation of IL is less than 10% of its maximum at that real part value. Furthermore, the worst cases where the insertion loss will be minimum only happen at certain $X_{s\min}$ values. This means that the same noise source impedance imaginary part will degrade the IL of the filter at different frequencies depending on the topology. There are methods to compensate this effect of the source impedance by impedance mismatching [8].

4 Method for Identifying Critical Frequency Ranges

The CM noise source impedance can be approximated by a series RLC network up to 30 MHz according to measurements of previous publications [9]. The value of the capacitance in the equivalent circuit is in the order of 10 nF which represents the parasitic capacitive coupling to the chassis ground. Here, it is chosen to be exactly 10 nF. The series inductance of the CM noise propagation path is in the 100 nH range, so it is set precisely to 100 nH. The resistance is a few ohms (1Ω) which is low enough for the imaginary part of the modeled source impedance (X_{sRLC}) to have an effect on the insertion loss according to Fig. 4. The load impedance is still assumed to be purely 25Ω . The resulting X_{sRLC} is plotted against frequency in Fig. 5 with a black line. The change from capacitive to inductive characteristic is clearly observable at the 5 MHz resonance frequency. The contour of the 3D surface that represents the insertion loss with the modeled source impedance at $R_{sRLC} = 1 \Omega$ is also plotted in the same plane. These projections can also be thought of as the edges of the surfaces whose contours are shown in Fig. 4 at all of the studied frequencies, as seen from the imaginary part. The insertion loss is indicated in percentage relative to the insertion loss measured in a 50Ω system, for example with a vector network analyzer (VNA). The negative values in dark red indicate that the studied filter will amplify the noise signal's amplitude at those frequencies, as can be seen from the negative values in Fig. 4 due to resonance. The values of

$X_{s\min}$ calculated by (7) for every frequency are also plotted with red dots. Discontinuities are visible here due to the discrete resolution of the frequency domain. The minimum of the insertion loss marked with dark red and increasingly darker blue corresponds well to the computed $X_{s\min}$ values. For every topology in Fig. 5, parasitics were included with the use of the expressions in (6). The values of the parasitics are as follows: $EPC_L = 10$ pF, $EPR_L = 10$ k Ω , $ESL_C = 1$ nH and $ESR_C = 100$ m Ω .

It can be observed from the plots that X_{sRLC} will deteriorate the insertion loss of the filter compared to its expected value differently for the topologies in the first column and the second column in Fig. 5. For the L, LC and LCL topologies in the first column, the IL has a steep minimum at a few 100 kHz at the intersection of X_{sRLC} and $X_{s\min}$. The IL of the LC topology takes its minimum at 525 kHz for example, but the critical frequency range determined by this point is relatively narrow, a few 100 kHz. This means that the IL of the LC topology will only be less than expected in the vicinity of the point determined by the intersection of X_{sRLC} and $X_{s\min}$. However, the topologies in the second column have a much wider critical frequency range, since X_{sRLC} overlaps with the area of low relative IL. For the CL topology, this means that between 650 kHz and 30 MHz approximately the IL will be less than expected from a VNA measurement.

Another study is shown in Fig. 6, using the proposed technique. The capacitances in the CLC (II) topology can also be asymmetric, not exceeding the maximum C_Y budget (200 nF in this case). Two scenarios were investigated regarding the values of C_1 and C_2 as in Fig. 3 (a). If the distribution of C_1 and C_2 is respectively 50 nF - 150 nF, the relative IL at around 260 kHz encounters a steep minimum, deteriorating the performance of the filter. On the other hand, if the distribution is 150 nF - 50 nF, the critical frequency range around 260 kHz is avoided, resulting in better attenuation. This is due to a resonance caused by the 10 μ H inductor and the series resultant capacitance of C_1 and C_2 (37.5 nF). In the second configuration, the damping of this resonance is greater, which results in higher insertion loss.

The presented graphical method can be used if the noise source impedance is not known exactly by measurement, only the approximate parameters in its equivalent circuit. These are much easier and faster to obtain, like the CM parasitic capacitance of the electric machine indicated in Fig. 1. With a baseline model for \bar{Z}_s , the frequency ranges can be predicted as described above where the IL will be less than expected, and also to what extent. Additional measures can be applied accordingly, for example choosing a different topology which has a narrower critical frequency range. Furthermore, the effect of a change in the parameters of the noise source impedance model can also be plotted and studied with the presented method. The parasitic capacitance for instance can change by orders of magnitude due to a modification for mechanical or thermal reasons. This way, responses to changes in the noise source impedance from EMC side can be made more effective and faster, which is important from the point of time-to-market.

5 Conclusion

The effect of the complex noise source impedance on the insertion loss of low-stage filter topologies used in the traction inverters of electric cars was studied. First, the relationship between the insertion loss and the termination impedances was established with the use of ABCD-parameters. Then, the calculation method for computing the extreme source impedance values at which the insertion loss will be minimum or maximum was overviewed. Exemplary results of this computation were shown with illustrations. Finally, a graphical method was proposed to identify critical frequency ranges at which the insertion loss will differ compared to its expected value measured in a 50 Ω system. The method can be used to tackle modifications affecting the termination impedance of the electromagnetic interference filter. Further improvements can be made to make the model on

which the method is based more accurate. Such is the inclusion of a more detailed representation of parasitic effects in order to extend the frequency range over which the method is applicable. Also, realistic noise sources need to be taken into account to make the EMC development of inverter filters even more efficient.

References

- [1] L. Tihanyi, *Electromagnetic Compatibility in Power Electronics*. IEEE Press, 1995.
- [2] L. Zhai, S. Yang, G. Hu and M. Lv, "Optimal design method of high voltage DC power supply EMI filter considering source impedance of motor controller for electric vehicle," in *IEEE Transactions on Vehicular Technology*, vol. 72, no. 1, pp. 367-381, 2023, <https://doi.org/10.1109/TVT.2022.3202528>.
- [3] K. S. Kostov and J. J. Kyyrä, "Insertion loss and network parameters in the analysis of power filters," in *Proceedings of the 2008 Nordic Workshop on Power and Industrial Electronics (NORPIE 2008)*, Espoo, Finland, 2008, 5 pages.
- [4] K. Kostov, J. Kyyrä, and T. Suntio, "Analysis and design of EMI filters for DC-DC converters using chain parameters," in *Proceedings of the 10th European Conference on Power Electronics and Applications (EPE 2003)*, Toulouse, France, 2003, 10 pages.
- [5] F. Luo, D. Boroyevich and P. Mattavelli, "Improving EMI filter design with in circuit impedance mismatching," *2012 Twenty-Seventh Annual IEEE Applied Power Electronics Conference and Exposition (APEC)*, Orlando, FL, USA, 2012, pp. 1652-1658, <https://doi.org/10.1109/APEC.2012.6166042>.
- [6] B. Audone and L. Bolla, "Insertion loss of mismatched EMI suppressors," in *IEEE Transactions on Electromagnetic Compatibility*, vol. EMC-20, no. 3, pp. 384-389, 1978, <https://doi.org/10.1109/TEM.1978.303666>.
- [7] R. Perrotta, "symlog" (<https://github.com/raaperrotta/symlog>), GitHub. Retrieved November 7, 2024.
- [8] F. Luo, D. Boroyevich, P. Mattavelli and H. Bishnoi, "EMI filter design considering in-circuit impedance mismatching," *2012 IEEE Energy Conversion Congress and Exposition (ECCE)*, Raleigh, NC, USA, 2012, pp. 4613-4618, <https://doi.org/10.1109/ECCE.2012.6342193>.
- [9] F. Fan, K. Y. See, X. Liu, K. Li and A. K. Gupta, "Systematic common-mode filter design for inverter-driven motor system based on in-circuit impedance extraction," in *IEEE Transactions on Electromagnetic Compatibility*, vol. 62, no. 5, pp. 1711-1722, 2020, <https://doi.org/10.1109/TEM.2019.2944663>.

Acknowledgements – We would like to thank the Robert Bosch Kft./Bosch Group, Hungary, for their professional support of the research that the study is based on. Project no. TKP2021-NVA-02 has been implemented with the support provided by the Ministry of Culture and Innovation of Hungary from the National Research, Development and Innovation Fund, financed under the TKP2021-NVA funding scheme.

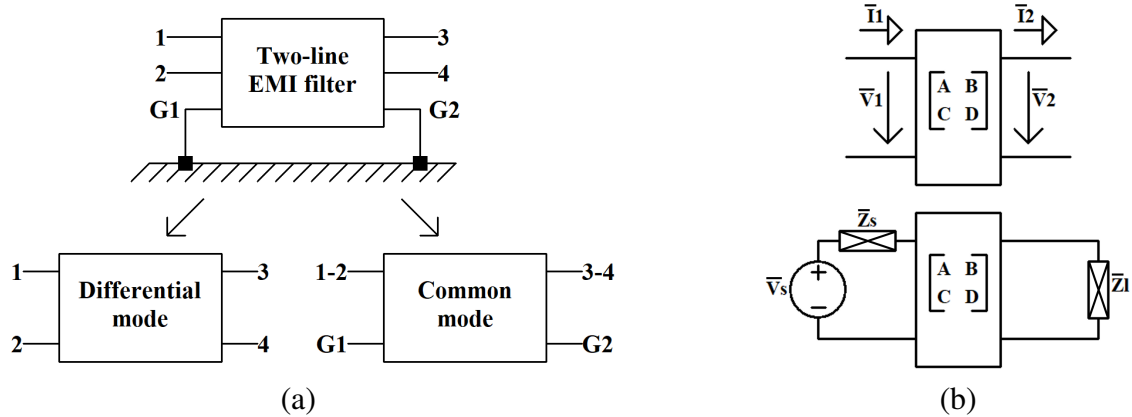


Figure 2: (a) Dividing the three-port EMI filter into two two-port networks. (b) Connecting the noise source impedance (\bar{Z}_s) and the load impedance (\bar{Z}_l) to the filter. The noise source (\bar{V}_s) is only for indication.

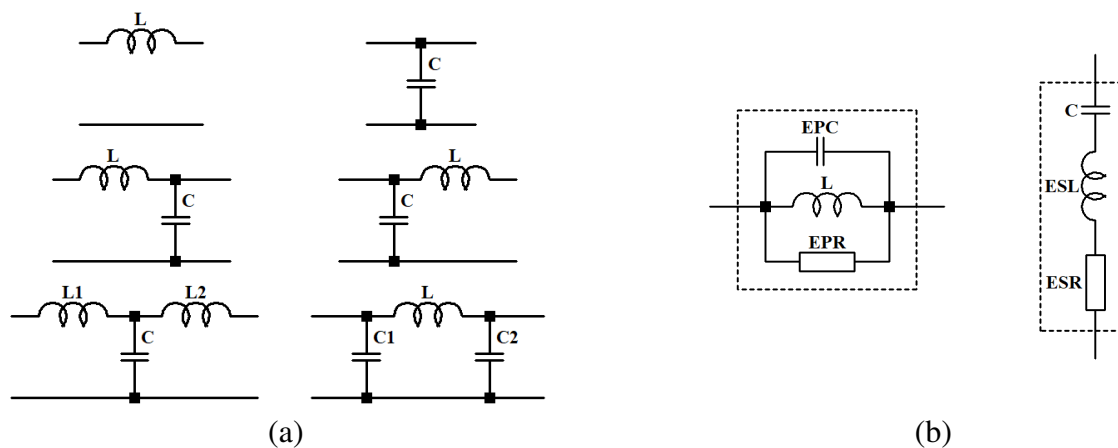


Figure 3: (a) The studied low-pass filter topologies: L, C, LC (T), CL (Γ), LCL (T) and CLC (II). (b) Models of the inductors and capacitors with parasitics.

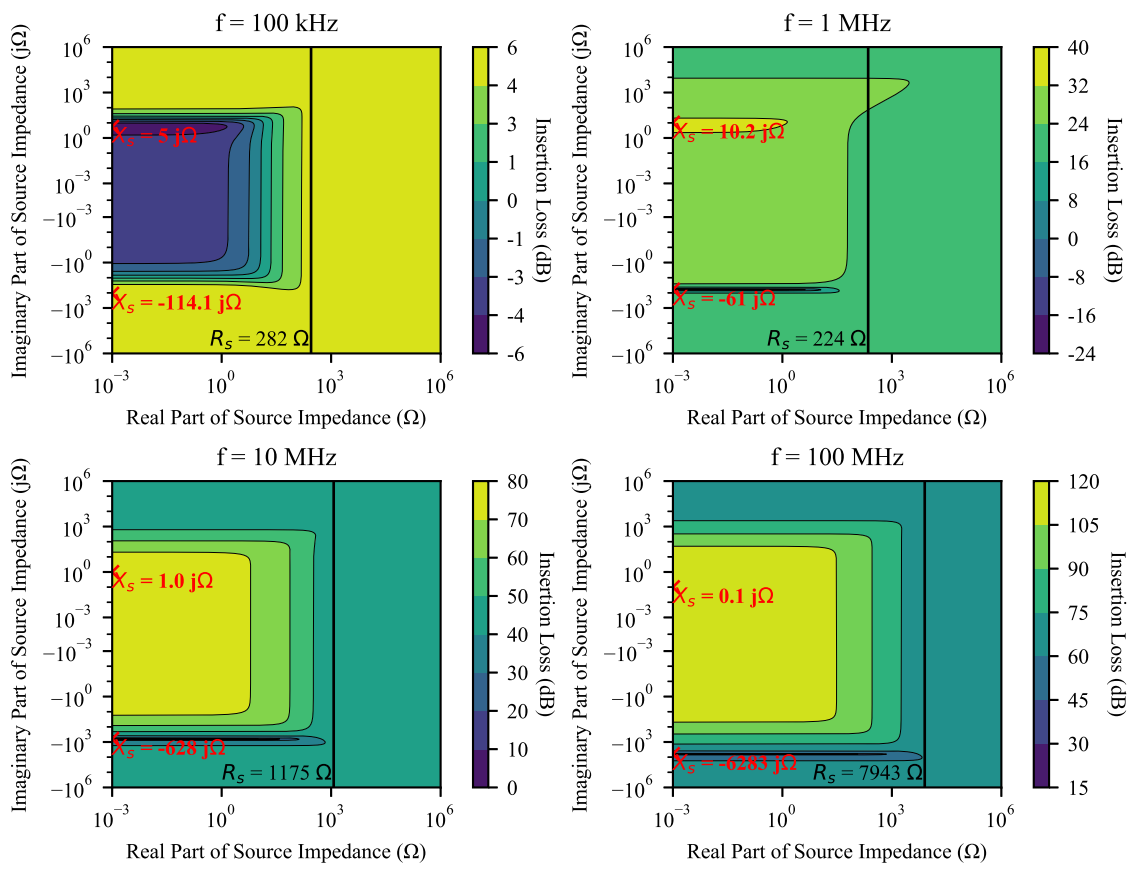


Figure 4: Variation of the insertion loss of an ideal LC topology ($L = 10 \mu\text{H}$, $C = 100 \text{ nF}$) as a function of the complex noise source impedance at different frequencies. The load impedance is $(25 + j0) \Omega$.

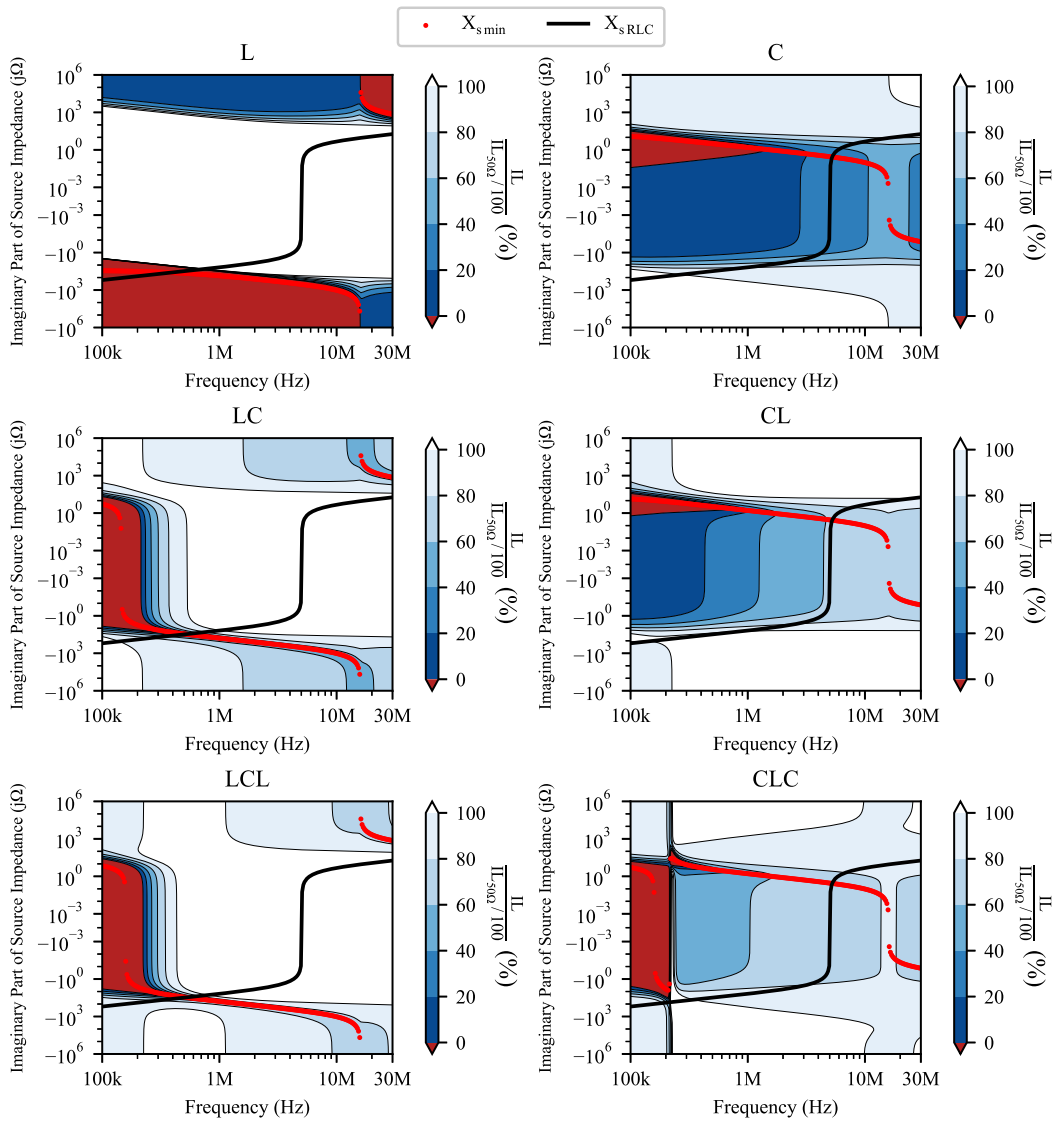


Figure 5: Contour of the insertion loss surface stretched by the frequency and the imaginary part of the noise source impedance.

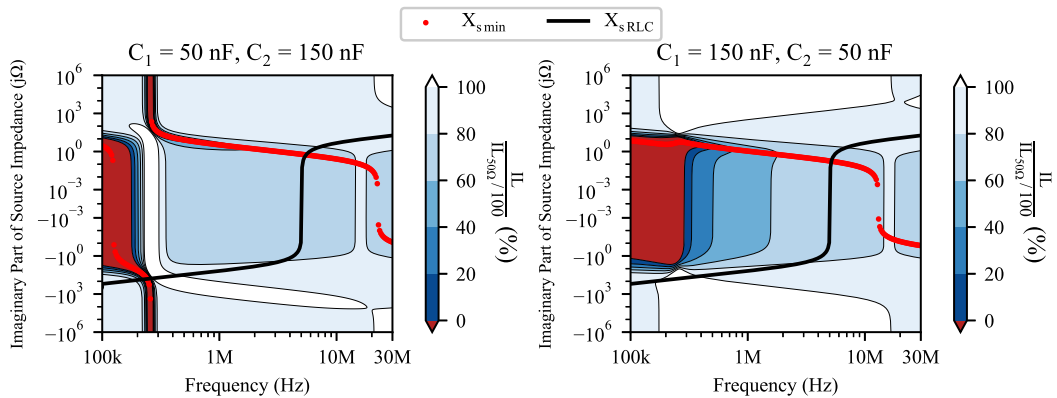


Figure 6: Changes in the critical frequency range for the CLC (II) topology with asymmetrical capacitances.